Cavity-enhanced second harmonic generation in a silica whispering-gallery microresonator

June 10, 2017

Centrosymmetric materials ... most significant application: surface probe... surface response is intrinsically weak, so several methods are used to enhanced surface SHG (e.g. plasmonic)... cavity boosts the intensity of light, making it a good platform for nonlinear optics...cavity enhanced SHG... Recently, SHG with bare silica cavity (Asano OL)...

Here, second harmonic, originating from symmetry breaking at the surface and bulk multipole response (fig.1 **b**), is observed under the continuous wave pump below 1 mW in a WGM microsphere made of centrosymmetric material. An unprecedented conversion efficiency of 0.049% W^{-1} benefits from doubly resonant enhancement of ultrahigh Q modes (phase-matching condition[also know as perfect phase matched]), which is achieved by thermal effect and optical Kerr effect. The work enriches the nonlinear toolbox of microcavity photonics and largely extends the emission range of silica microresonators with ultralow pump power, making it possible to push the frequency conversion process down to the quantum regime[refs in Asano OL]. More significantly, the fruitful surface SHG and SFG detection methods can be introduced into (bridged with?) the sensitive microcavity sensing, which enables surface-specific detection with low pump power and high sensitivity.

In the experiment, a silica microsphere (diameter $\sim$ 62 μm) is pumped through a tapered optical fiber (waist diameter $\sim$ 1 μm) at 1550 nm band [1, 2], as shown in fig.1 **a**. To collect SH signal efficiently, a second fiber taper (waist diameter $\sim$ 0.5 μm) designed for 780 nm band is incorporated into the system. The intrinsic quality factor (Q) for the pumped cavity mode is 4.8×10^7. Figure 1**c** shows a typical SH spectrum from the electron-multiplying CCD (EMCCD) and the corresponding pump spectrum from the optical spectrum analyzer (OSA). The SH signal of 777.75 nm appears when pumped at 1555.14 nm, which deviates only 0.023% from the expected wavelength, falling into the resolution tolerance of OSA and EMCCD. Note that stimulated Raman scattering and parametric oscillation do not occur because their thresholds are far above the pump power in the experiment. Third harmonic generation is also absent due to the phase mismatch in the nonlinear optical process. Moreover, SH signals arise in the full range when cavity modes are pumped from 1545 nm to 1565 nm, as shown in Fig.1d. Among the occurrence of SH, a maximum signal power of 5 nW can be obtained via the signal fiber. To compare the collecting efficiency of the two fibers, we optimize the fiber-cavity coupling so that the SH signal from the pump fiber is also observable but the maximum power is still over one order of magnitude weaker than that from the signal fiber. From either fibers, SH signal is absent when the pump is off-resonance with cavity modes, which helps to eliminate the possibility of spurious signals such as the second order diffraction of the EMCCD grating.

The doubly resonant enhancement plays a pivotal role in efficient SHG, which is achieved by perfect phase-matching including momentum conservation and energy conservation. The former can be fulfilled by a pair of modes with proper angular momentum relation $m_2 = 2m_1$, where m_1 (m_2) is the angular number of the pump (SH) cavity mode. However, the material and geometric dispersion presents a challenge on energy conservation, obstructing the double resonance $\omega_2 = 2\omega_1$ and consequently, efficient SHG. More accurately, the SH power can be derived from coupled mode equations (see Supplementary Information)

$$P_2 = \frac{4|g|^2 Q_2^2/(\omega_2 Q_{1e})}{4Q_2^2(2\omega_p/\omega_2 - 1)^2 + 1} \frac{16Q_1^4 P_1^2/(\omega_1 Q_{2e})^2}{[4Q_1^2(\omega_p/\omega_1 - 1)^2 + 1]^2}, \tag{1}$$

where the subscripts 1, 2 represent the pumped mode and SH mode respectively. ω_i is the mode frequency and ω_p is the pump frequency. P_1 denotes the input pump power, g is the coupling coefficient between two modes, Q_i ($i = 1, 2$) stands for the loaded quality factor and Q_{ie} represents the external quality factor. The pump power depletion is ignored due to the weak second order nonlinear effect in silica. Eq. (1) shows that ultrahigh Q is indispensable in boosting the SH power, while it also presents a challenge in double resonance by magnifying the frequency mismatch induced by the material and geometric dispersion. In order to compensate the dispersion, SH modes with higher order radial number was proposed or used [3][Levy], which relies on delicate geometric design of the cavity. In the experiment, however, the desired phase-matching can be disturbed by the deviation of cavity from its designed geometry, making one of the mode off-resonance and impeding highly efficient SHG. Therefore, to tune the cavity dispersion precisely and dynamically, we propose and experimentally realize a versatile method, leveraging mode frequency shift induced by thermal behavior (namely thermal expansion, thermally induced refractive index change and the optical Kerr effect) [4, 5].

The mechanism of thermal and Kerr assisted phase matching process is illustrated in fig.2a. When the pump power is weak and the mode frequency shift is negligible (cold cavity), the pumped (ω_{10}) and SH modes (ω_{20}) usually cannot be on resonance with the pump light and its SH simultaneously. With a larger input

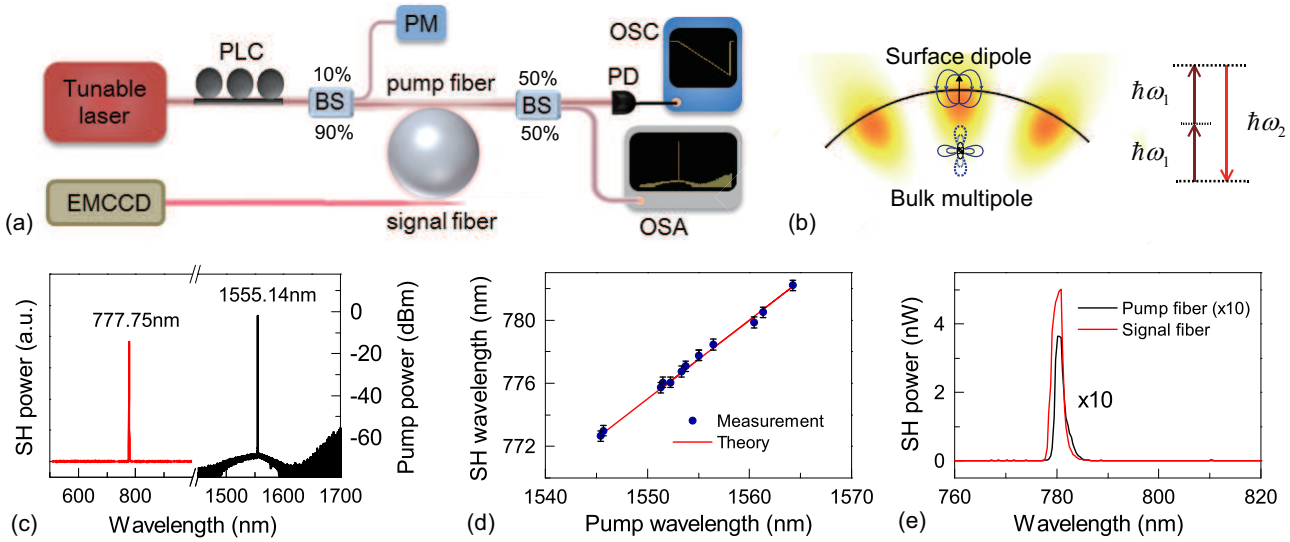

Figure 1: **Experimental set-up and observation of cavity-enhanced SH signals. a,** The pump light from a tunable laser around 1550 nm is coupled into a silica microsphere through a tapered fiber, and a second fiber is used to collect the SH signal. OSC: oscilloscope. OSA: optical spectrum analyzer. PLC: polarization controller. BS: beam splitter. EMCCD: electron-multiplying CCD. **b,** SH is generated from the surface dipole response and the bulk multipole response in a WG microsphere. **c,** Measured SH spectrum (red) and the corresponding pump spectrum (black). **d,** Measured SH wavelengths versus the corresponding pump wavelengths when different modes are pumped. **e,** Comparison of SH power collected by signal fiber and pump fiber (10 times magnified).

power, the pump mode experiences a red shift due to xxx: $\omega_1 = \omega_{10} - B_{11}|\alpha_1|^2$, where $|\alpha_1|^2$ is the intra-cavity power of the pumped mode and B_{11} is the coefficient of pump frequency shift. In this case, the wavelength of pump light should also increase to catch the pump mode, resulting in the non-Lorentzian, triangular transmission shape [carmon2004]. The SH mode also exhibits a red shift from cold cavity frequency, which can be described by $\omega_2 = \omega_{20} - B_{12}|\alpha_1|^2$ where B_{12} is the coefficient of SH frequency shift. The thermal and Kerr effects of the SH is ignored in the analysis. In the process of tuning pump frequency from the cold cavity mode to resonance, the larger rate of red shift for the SH of pump light ($\omega_p/2$) helps it to catch the SH mode (ω_2) at a certain pump-cavity detuning where the phase-matching condition is fulfilled the SH power reaches a peak value (state 2 in fig.2a). Due to the ultrahigh Q of the SH resonance, the SH power diminishes rapidly before and after reaching the on-resonance pump frequency (state 1 and 3 in fig.2a and b). xxx phase matching can also be realized in other cases with different rate of SH mode frequency shift or initial detuning between $\omega_p/2$ and ω_2 (see SI).

As shown in fig. 2c, the SH power is measured by varying the pump wavelength in the detuning range of the gray area in fig. 2b with a fixed input power of 4.46 mW. [fitting results here]

[Fitting] The critical input power is fitted to be 832.5μW and the corresponding SH power is fitted to be 381pW. Eq.(1) and $\omega_1 = \omega_{10} - B_{11}|\alpha_1|^2$ [6], $\omega_2 = \omega_{20} - B_{12}|\alpha_1|^2$ are used to fit the experimental data, where ω_{i0} is the mode frequency in the cold cavity, $|\alpha_1|^2$ is normalized to the intra-cavity power of the pumped mode and B_{1i} is the coefficient of intra-cavity power induced frequency shift. The parameters related to the pumped mode can be extracted from the measurements. Increasing the input power leads to the appearance and broadening of the for the pump[6], resulting from the mo

The dependence of SH power on power pump is also studied, as shown in fig.2d. At each input power, we search for the maximum SH output power in the wavelength range from the cold cavity mode (1555.02nm) to the pump on-resonance wavelength. Among different values of input power, a critical power manifests itself, at which the SH power reaches the peak value just before the pump light becomes on resonance and then thermally unlocked. In this case, the pump light and its SH achieve double resonance simultaneously, which represents the most efficient SHG with the pump power of 879 μW and the conversion efficiency of 0.049% W^{-1}. Below the critical input power, the SH of pump light is off resonance when the pump is still thermally locked in the mode, which largely weakens the SH power. Above the critical power, the increasing input power shifts the pumped mode more to the red side (the pump is not completely on resonance) and lowers the enhancement of the pump light, which counteracts with the increasing input power and makes the intracavity power almost unchanged at the SH resonant detuning. Consequently, the SH power remains the same with increasing input power.

[where?] In the THG experiments in silica microresonators[7, 8], the phase mismatch curve is flat for high order radial modes, and the shift speed of the pump TH frequency and the TH frequency mode may be similar. Consequently, the high order radial modes induced phase matching may play a major role so that the P_1^3 relation can be observed. Microresonator SHG in other materials usually use different phase matching strategy to achieve broad band or tunable phase matching, e.g. quasi-phase-matching [cite more later]...The quality factor is also moderate so that the thermal effect and Kerr

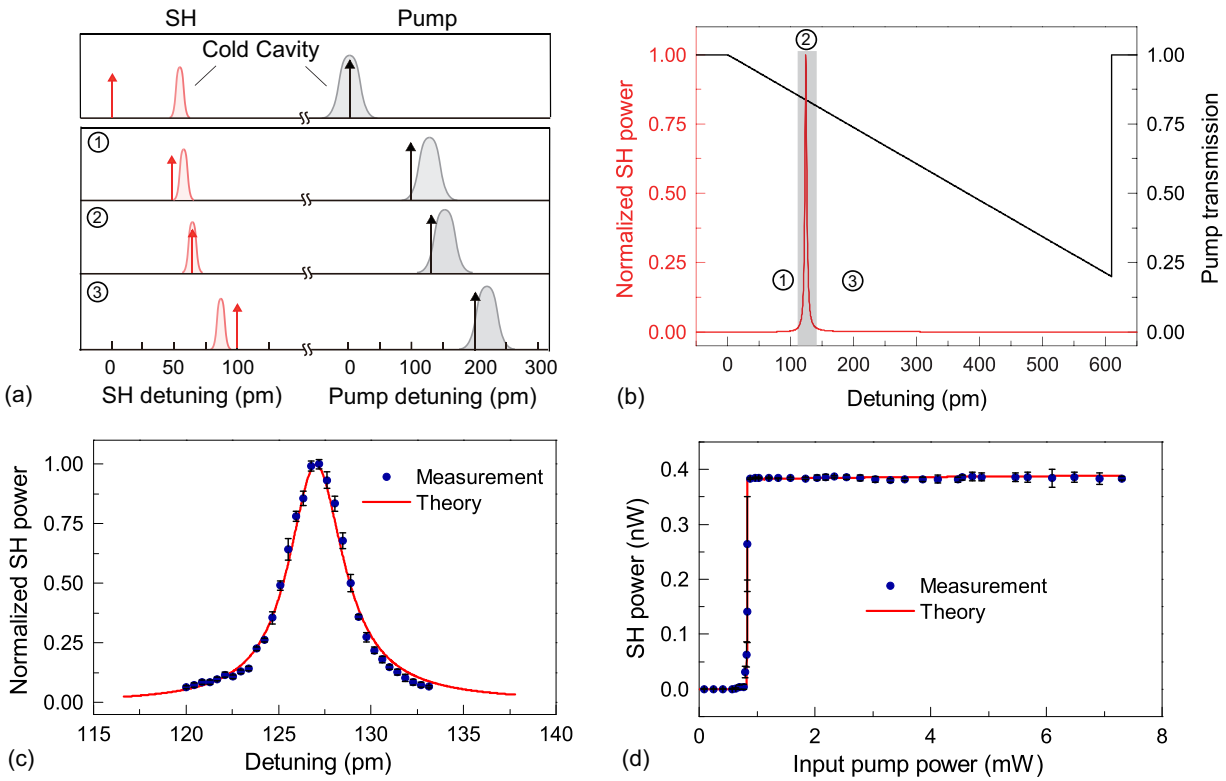

Figure 2: **Thermal effect and Kerr effect assisted phase-matching.** **a,** Schematic of the phase-matching process. Detuning here is the wavelength relative to the cold-cavity wavelength of the pumped mode (to half of this wavelength for SH detuning). The black (red) arrow represents the detuning of the pump light (its SH). The gray (red) Lorentzian line represents the pumped mode (SH mode). 1-3 show three states with increasing pump wavelength but the same input power. **b,** Normalized SH power and the pump transmission at different pump wavelength detuning. 1-3 correspond to the three states in panel **a**. The gray area is enlarged in panel **c** as the theoretical red line. **c,** SH power versus pump detuning with the input power of 4.46mW. **d,** The dependence of maximum SH power at all the pump detuning on the input power.

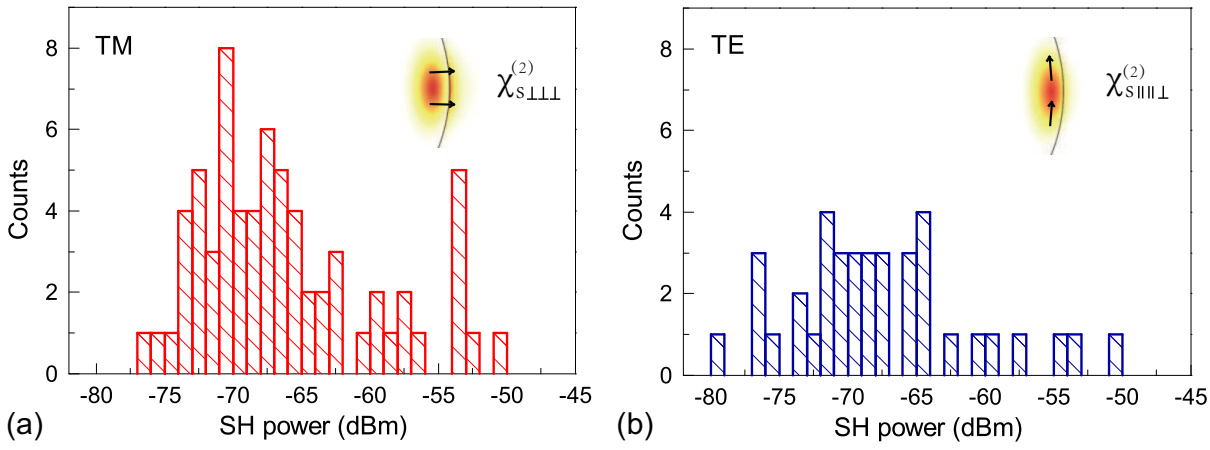

Figure 3: **SH power histogram with different pump polarization.** **a,** TM and **b,** TE modes are pumped to generate SH respectively. Insets: Field amplitude distribution and the direction of the electric field (black arrow).

effect do not manifest themselves in the SHG process.

It is also possible to measure the explicit $P_2 \propto P_1^2$ dependence by introducing another degree of freedom to manipulate the SH mode frequency. For example, a control light can be coupled into another mode to change the intra-cavity power and thus achieving the double on-resonance condition at various input pump power. The specific measurement plan is beyond the scope of this [letter?] and is still under investigation.

Apart from the unique power dependence, the SH

power enhanced by the microresonator also exhibits a polarization dependence. The polarization of the pump light is adjusted so that transverse magnetic (TM) or transverse electric (TE) modes from 1545 nm to 1565 nm are pumped. The maximum SH power of each SHG process is recorded for the two polarization respectively, as shown in the histogram in 3. After searching for SH in the wavelength range three times with each polarization, a total number of 69 (40) SHG incidence is recorded for TM (TE) polarization, and the average SH power is 0.843 nW (0.619 nW). The dependence on polarization originates from the polarization dependent nonlinear coupling coefficient g in eq.(1), which bridges the microresonator with the second order nonlinearity of centrosymmetric material.

Using the Helmholtz equation and the relation between electric field and nonlinear polarization, the coupling coefficient induced by surface nonlinear response can be derived as

$$g_{s0} = 2i\frac{\omega_1^2}{\omega_2 n^2}\frac{\int_{\text{surface}} \mathbf{E}_{02}^* : \chi_{s0}^{(2)} : \mathbf{E}_{01}\mathbf{E}_{01}\mathrm{d}\mathbf{S}}{\int |\mathbf{E}_{02}|^2 \mathrm{d}\mathbf{V}} \qquad (2)$$

where n is the refractive index, $\chi_s^{(2)}$ is the surface nonlinear susceptibility, and $\mathbf{E}_{0i}(\mathbf{x})$ is the normalized electric field so that $\alpha_i\mathbf{E}_{0i}(\mathbf{x})$ represents the complete electric field.

The bulk multipole nonlinear polarization can be written as $\mathbf{P}_\gamma = \gamma\nabla(\mathbf{E}\cdot\mathbf{E})$ and $\mathbf{P}_\delta = \delta(\mathbf{E}\cdot\nabla)\mathbf{E}$, where γ and δ are the nonlinear coefficients. The first term represents a longitudinal wave and can couple with the SH only at the surface. Therefore it can be incorporated into an effective surface susceptibility $\chi_s^{(2)} = \chi_{s0}^{(2)} + \chi_{s,\gamma}^{(2)}$[9]. The coupling coefficient induced by the second term can be written as

$$g_b = 2i\frac{\omega_1^2}{\omega_2 n^2}\frac{\int \delta\mathbf{E}_{02}^* \cdot (\mathbf{E}_{01}\cdot\nabla)\mathbf{E}_{01}\mathrm{d}\mathbf{V}}{\int |\mathbf{E}_{02}|^2 \mathrm{d}\mathbf{V}} \qquad (3)$$

The total coupling coefficient between the two modes is $g = g_s + g_b$.

There are three non-zero components $\chi_{\perp\perp\perp}$, $\chi_{\parallel\parallel\perp}$ and $\chi_{\perp\parallel\parallel}$ in the surface second order susceptibility tensor of fused silica. $\chi_{\perp\perp\perp}$ ($\chi_{\parallel\parallel\perp}$) plays a major role when TM (TE) mode is pumped. $\chi_{\perp\parallel\parallel}$ can be ignored in studying SHG due to the non-degeneracy of TM and TE modes. TM modes are preferable in surface induced SHG because $\chi_{\perp\perp\perp}$ is nearly an order of magnitude larger than $\chi_{\parallel\parallel\perp}$ [10]. The amplitude of bulk nonlinear response g_b relies on the specific field distribution in the microsphere. Note that for a TE mode, the divergence is along the polar direction, which exhibits geometric symmetry with regard to the equatorial plane. If both the pumped mode and the SH mode are fundamental in the polar direction (polar number l = azimuthal number m), g_b vanishes due to the divergence and the polar symmetry. Because of a better confinement in the radial direction and thus a larger divergence for most of the modes, TM modes tend to have a larger g_b than TE modes. For example, in a silica microsphere with a diameter of 62μm, the TM pumped mode with $l_1 = m_1 = 171$ and its SH mode with $l_2 = m_2 = 342$ produces a g_b 18 times larger than that of the TE mode with $l_1 - 1 = m_1 = 171$ and its SH mode with $l_2 - 1 = m_2 = 342$ (in both cases, the radial numbers of the pumped mode and SH mode are 1 and 2 respectively due to phase matching considerations).

The polarization dependence can be utilized to add to the surface specificity for SHG sensing. Mediated by $\chi_{\parallel\parallel\perp}$, two TE polarized photons can generate a TM polarized photon. For nonlinearity from bulk multipole effects (g_b), TE polarized pump can only generate TE SH. In this case, the bulk response can be eliminated and thus restricting the SHG on the surface.

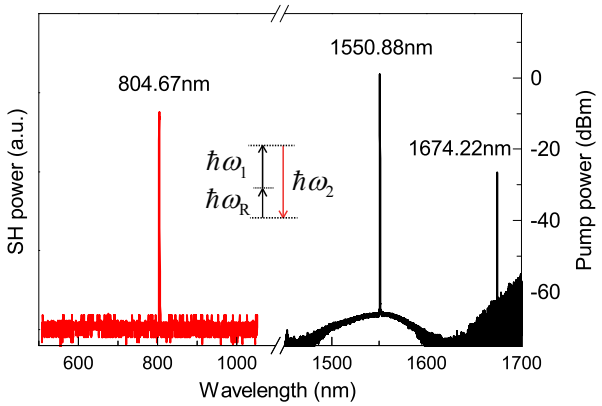

Figure 4: **Measured spectra of second-order sum frequency generation (SFG).** The pump light (ω_1) and Raman light (ω_2) are summed to generate the SF signal (ω_3).

Sum frequency generation (SFG) can also take place when the pumped mode produce a Raman signal. Shown in fig.4b is an SF signal (804.67 nm) and the corresponding pump (1550.88 nm) and its Raman signal (1674.22 nm) with an input power of 7.33 mW, which is above the Raman threshold for this mode. The deviation of the SF wavelength from the expected value (804.63 nm) is much smaller than the resolution of EMCCD.

[Conclusion]

References

[1] J Cheung Knight, G Cheung, F Jacques, and TA Birks. Phase-matched excitation of whispering-gallery-mode resonances by a fiber taper. *Optics letters*, 22(15):1129–1131, 1997.

[2] Ming Cai, Oskar Painter, and Kerry J Vahala. Observation of critical coupling in a fiber taper to a silica-microsphere whispering-gallery mode system. *Physical review letters*, 85(1):74, 2000.

[3] Gregory Kozyreff, JL Dominguez Juarez, and Jordi Martorell. Whispering-gallery-mode phase matching for surface second-order nonlinear optical processes in spherical microresonators. *Physical Review A*, 77(4):043817, 2008.

[4] Pascal DelHaye, T Herr, E Gavartin, ML Gorodetsky, Ronald Holzwarth, and Tobias J Kippenberg. Octave spanning tunable frequency comb from a microresonator. *Physical Review Letters*, 107(6):063901, 2011.

[5] T Herr, V Brasch, JD Jost, CY Wang, NM Kondratiev, ML Gorodetsky, and TJ Kippenberg. Temporal solitons in optical microresonators. *Nature Photonics*, 8(2):145–152, 2014.

[6] Tal Carmon, Lan Yang, and Kerry J Vahala. Dynamical thermal behavior and thermal self-stability of microcavities. *Optics Express*, 12(20):4742–4750, 2004.

[7] Tal Carmon and Kerry J Vahala. Visible continuous emission from a silica microphotonic device by third-harmonic generation. *Nature Physics*, 3(6):430–435, 2007.

[8] D Farnesi, A Barucci, GC Righini, S Berneschi, S Soria, and G Nunzi Conti. Optical frequency conversion in silica-whispering-gallery-mode microspherical resonators. *Physical review letters*, 112(9):093901, 2014.

[9] Tony F Heinz. Second-order nonlinear optical effects at surfaces and interfaces. *Nonlinear surface electromagnetic phenomena*, 29, 1991.

[10] Francisco J Rodriguez, Fu Xiang Wang, and Martti Kauranen. Calibration of the second-order nonlinear optical susceptibility of surface and bulk of glass. *Optics express*, 16(12):8704–8710, 2008.